ADVANCED ELECTRONIC MATERIALS
www.advelectronicmat.de

Photothermal-Induced Nanowelding of Metal–Semiconductor Heterojunction in Integrated Nanowire Units

*Pintu Ghosh, Jinsheng Lu, Ziyao Chen, Hangbo Yang, Min Qiu, and Qiang Li**

An improvised and comparatively inexpensive method for welding semiconductors and metal nanowires (NWs) utilizing a plasmon-enhanced photothermal effect is presented in this article. Different types of heterojunction-based (single Schottky junction and back-to-back Schottky junctions) electronic nanodevices are fabricated by welding various combinations of silver and ZnO NWs on two gold electrodes using continuous wave laser ($\lambda = 532$ nm) shots. It is inferred from the current–voltage characteristic curves of these devices that the junction formed between the ZnO nanowire (NW) and the gold electrode demonstrates Schottky barrier-like behavior, whereas the junctions between silver-and-gold and silver-and-ZnO behave like ohmic contacts. The maximum currents obtained for a single Schottky junction and back-to-back Schottky junctions corresponding to the applied bias voltage 40 V are 42 µA and 7 µA, respectively. This plasmon-enhanced nanowelding technique extends the range of applications of nanowelding in fabrication of electronic nanodevices.

1. Introduction

Toward further downsizing and accomplishing high-performance, 1D semiconductor and metal heterojunction-based electronic nanodevices are emerging as an appealing supplement to the existing Si-technology.[1,2] In this regard, zinc oxide (ZnO) nanowire (NW) is of particular interest. Owing to its unique electrical, optical, and mechanical properties, such as large direct bandgap (3.37 eV), piezoelectricity, and pyroelectricity,[3] it finds diverse applications, including field effect transistor,[4] field emission device,[5] nanogenerator,[6] UV laser,[7,8] light emitting diode,[9] sensor,[10] and solar cell.[11] On the other hand, silver (Ag) NW exhibits prominent surface plasmon resonance and low resistance, which helps in improving the nanowire junction conductance, and therefore it finds applications in various optoelectronic devices, including flexible displays, solar cells, and transparent conducting electrodes.[12–15] However, to utilize ZnO and Ag nanowires (NWs) in various heterostructure-based 1D electronic nanodevices, it is important to develop an adequate method to combine them together and understand its charge transport mechanisms.

Recent advancements in the field of welding of NWs research indicate its potential capabilities in fabrication and repairing nanoelectronics,[16–19] nanophotonics,[20] nanomedicine,[21] and nanoelectromechanical systems.[22] There are reports of successful nanowelding following various techniques, including thermal annealing,[23] optical welding,[24–28] capillarity-driven welding,[29] chemical welding,[30] spot welding,[31] stretch-induced cold-welding,[32–34] and welding by Joule heating.[35,36] Although much progress has been achieved in this field, there remains many cumbersome issues, such as necessitating complicated and expensive experimental setup, use of chemicals which can contaminate the system, and lack of robustness corresponding to mechanical strength and electrical connectivity, yet to be addressed. Furthermore, the joining of semiconductor and metal NWs remains a challenging issue for miniaturization and integration of next generation nanodevices as the melting points of these two different types of materials are different.

In this article, we present a relatively simple technique to achieve adequate welding of ZnO NW with Ag NW and also both type of NWs with Au electrode toward realizing heterojunction-based electronic nanodevices. The effects of local heat generation in closely spaced semiconductor and metal nanostructures due to strong optical interactions have been utilized for melting and eventually welding these nanostructures. Following this technique, four different electronic devices (two devices consisting of one Schottky and two ohmic junctions, one device with two back-to-back Schottky junctions, and another one with three ohmic contacts) have been fabricated. The devices with one Schottky and two ohmic junctions have been fabricated following two different approaches for two different orientations of the ZnO (top/bottom) and Ag (bottom/top) NWs. Although the temperature difference between the melting points of ZnO and Ag NWs is about 1000 K, it has been demonstrated that the melting points of both NWs are reached simultaneously when ZnO NW in on top of Ag NW, which results in superior quality of welding. Thereafter, toward understanding the transport mechanisms of all these devices, the obtained current–voltage (I–V) characteristic curves are analyzed in detail. This photothermal nanowelding technique paves the path for realizing heterostructure-based 1D electronic nanodevices.

Dr. P. Ghosh, J. Lu, Z. Chen, Dr. H. Yang, Prof. M. Qiu, Prof. Q. Li
State Key Laboratory of Modern Optical Instrumentation
College of Optical Science and Engineering
Zhejiang University
310027 Hangzhou, China
E-mail: qiangli@zju.edu.cn

The ORCID identification number(s) for the author(s) of this article can be found under https://doi.org/10.1002/aelm.201700614.

DOI: 10.1002/aelm.201700614

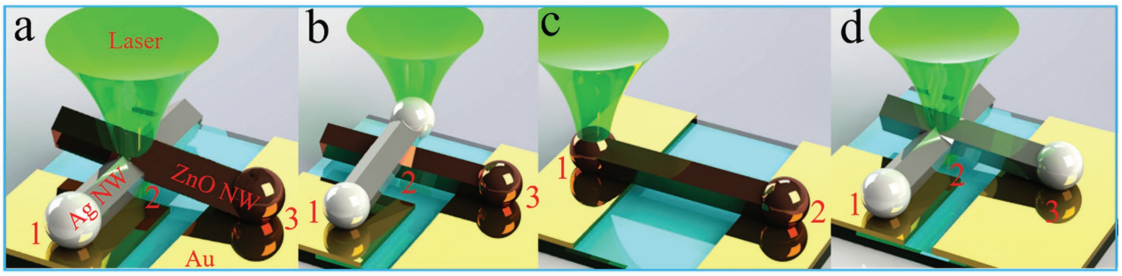

Figure 1. Schematic model diagrams of the four fabricated devices. Depiction of the welding process by a focused CW laser beam (λ = 532 nm). Welding of the junction of an Ag NW and a ZnO NW when a) ZnO NW is kept on top of Ag NW, and while b) Ag NW is kept on top of ZnO NW. c) Welding of two ends of a ZnO NW on two different Au electrodes. d) Welding of the junction of two Ag NWs. The numbers (1, 2, and 3) represent the welded junctions.

2. Results and Discussion

Optical energy is converted to thermal energy when surface plasmon polaritons are excited on the metal NW or semiconductor NW absorbs focused continuous wave (CW) laser light. This thermal energy increases the temperature of the metal and semiconductor nanowires, which in turn melts these NWs when the temperature of the materials crosses their respective melting points. The schematic diagrams of this photothermal-induced nanowelding technique toward fabricating different types of electronic nanodevices are shown in **Figure 1**. Toward realizing electrical contact between metal and semiconductor NWs, two different approaches, which are presented in the subsequent sections, have been persuaded.

2.1. Nanowelding with ZnO Nanowire on Top

The laser beam power plays a crucial role to obtain optimized welding of the junction of the NWs. If the power is too less, none of the NWs melts and results in poor quality of welding (current through the device is less than a few nA corresponding to the applied voltage ranging from −40 to 40 V). On the other hand, too high power destroys both the NWs. The optimum incident laser beam power (P) for welding depends on polarization of the laser beam, orientation of the NWs and also on length (L) and diameter (D) of the NWs.

The electronic nanodevices are fabricated following a series of steps described below. First, a ZnO NW (D = 302 nm) is placed on top of an Ag NW (D = 244 nm) in such a way that they make a plus sign and one end of each of the NWs is on a different Au electrode. The length of both the NWs is about 10 µm. These two NWs are welded at three different places: Ag NW on Au electrode, Ag and ZnO NW junction, and ZnO NW on Au electrode. Figure 1a shows the schematic model diagram of the experimental setup, and the above mentioned three points are marked as 1, 2, and 3, respectively. Focused CW laser (λ = 532 nm) shots are used for welding. Laser shot duration, which is controlled by a mechanical shutter, is kept fixed at 4 ms for all experiments. A microscope objective (100×) is used for tight focusing (beam waist is about 400 nm) of the laser beam. The sample is placed on a nanometer scanning stage for precisely targeted welding. The complete experimental setup depicting the welding technique is shown in Figure S1 of the Supporting Information, and more details about the experimental procedures are provided in the Experimental Section. To weld the junction of the Ag and ZnO NWs, parallel polarization (electric field parallel to the top ZnO NW) of the incident laser beam with power 55 mW is used. Parallel polarization of the incident laser beam is chosen as it provides better control over the welding process compared to perpendicular polarization (electric field perpendicular to the top NW). The details regarding the selection of parallel polarization can be found in Section 2 of the Supporting Information (see also Figure S2, Supporting Information). The SEM image of the welded junction of the NWs is shown in **Figure 2**a.

It is observed from the simulated results that the maximum temperatures of the ZnO and Ag NWs at the focal point of the laser are about 2200 and 1200 K, respectively (see Figure 2b,c). These temperatures are close to the melting points (T_m) of bulk Ag (T_{mAg} = 1234.95 K)[37] and bulk ZnO (T_{mZnO} = 2248.15 K),[38] and therefore both the NWs melt and join together (contact point gets converted to area as both the NWs broaden due to melting) for this incident laser power and polarization. In this regard, it can be mentioned that the melting point decreases with diameter of the NWs, but the effect is less prominent as the diameter is more than a few tens of nm.[39] The simulated results show that the incident laser polarization for which the electric field is parallel to the top NW is more favorable (see Section 2, Supporting Information), and the required laser power for welding increases with length and diameter of the NWs (see Section 3, Supporting Information).

It has been observed that the current cannot be measured if only the junction of the NWs is welded and the NWs are not welded on the Au electrodes. Therefore, the other ends of the NWs are also welded on the Au electrodes (see Figure 1a). Parallel polarization of the incident laser (P = 70 mW) beam is used to weld ZnO NW on Au electrode. For this incident laser power and polarization, the temperature of the contact point of the ZnO NW and Au substrate reaches about 2200 K (Figure S4a, Supporting Information), therefore both Au substrate and the ZnO NW melt, and the welded junction is realized (see Figure 2d). The details about the welding of Ag NWs on Au substrate are also provided in Section 4 and Figure S4 of the Supporting Information.

After welding the NWs at three places as shown in Figure 1a, current–voltage (I–V) characteristic curves are obtained using a picoammeter. The experimental setup for electrical

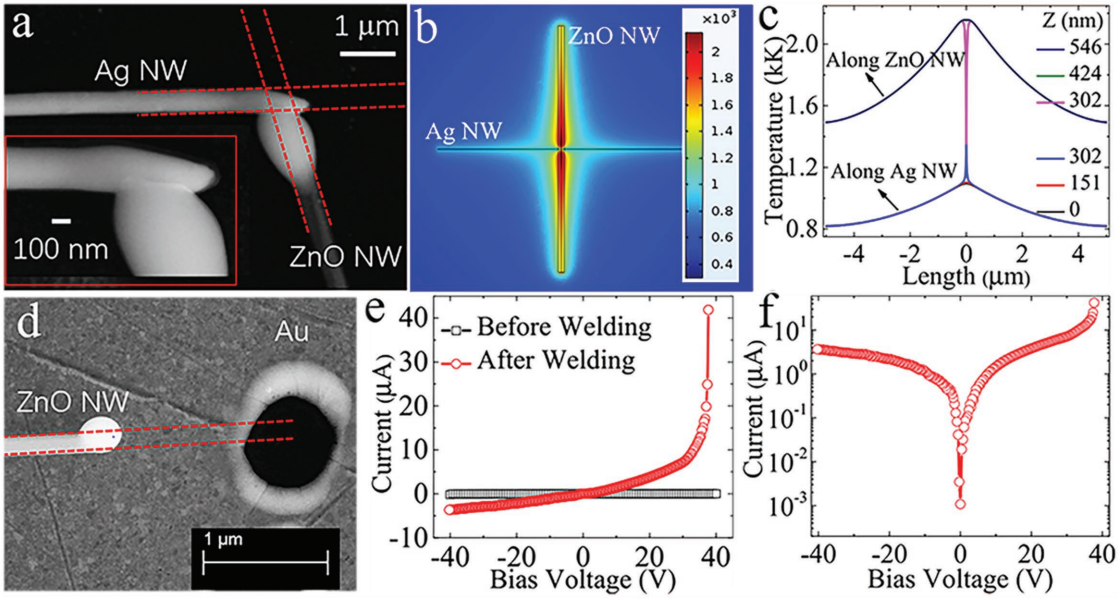

Figure 2. Welding of Ag and ZnO NWs with ZnO NW on top. a) SEM image of the welded junction of the NWs. The inset shows the zoomed in image of the junction. b) 2D plot of temperature distribution for $Z = 302$ nm. The color bar shows temperature in Kelvin (K) scale. c) Line plots of temperature distribution along the NWs at different height from the top surface of the Au electrodes ($Z = 0$). Both (b) and (c) plots are obtained from COMSOL simulation corresponding to parallel polarization (electric field parallel to ZnO NW) of the incident laser beam ($P = 55$ mW). d) SEM image of the welded junction of ZnO NW on Au electrode. e) Current–voltage characteristic curve for the welded system. The curve obtained for the before welding system is also plotted for comparison. f) Semilog plot of current–voltage characteristic curve. The dotted red lines represent the initial (before welding) orientation of the NWs.

measurement technique is shown in Figure S1 of the Supporting Information. The comparison of the *I*–*V* characteristic curves obtained for the before and after welding systems show that the current value increases drastically after welding (see Figure 2e). The maximum current value obtained for this device corresponding to a maximum applied bias voltage 40 V is 42 μA. Furthermore, the *I*–*V* curve exhibit rectifying characteristics indicating formation of Schottky barrier. Owing to the high vacuum work function (Φ) of Au ($\Phi_{Au} \approx 5.3$ eV),[40] it is expected to form a depletion layer at the interface of the welded junction of Au thin film and the n-type ZnO NW,[41,42] and therefore it is more likely to act like Schottky barrier.[43] The Schottky barrier height (SBH), which is based on the vacuum work function of the metal relative to the vacuum electron affinity (χ) of the semiconductor ($\Phi_B \approx | \Phi_{metal} - \chi_{SC} |$), corresponding to Au–ZnO junction is expected to be higher compared to Ag–ZnO junction owing to the higher Φ value of Au compared to Ag ($\Phi_{Ag} \approx 4.4$ eV).[40,44] Therefore, the SBH corresponding to Au–ZnO junction is speculated to play a predominant role in determining the rectifying behavior. The weak rectification is attributed to the lowering of Schottky barrier height Φ_B due to Fermi level pinning and Schottky effect.[45] The logarithmic plot of current–voltage characteristic curve for the welded system shows distinguishably different current profile for change of bias voltage polarity (see Figure 2f).

Toward understanding the charge transport mechanism of the device, the *I*–*V* characteristic curve corresponding to the forward bias voltage is plotted in log scale (see **Figure 3**a). It

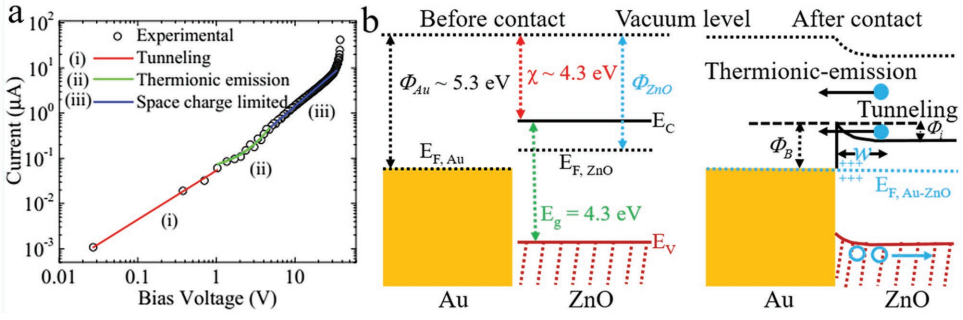

Figure 3. Electrical properties of the welded junctions. a) Logarithmic plot of current–voltage characteristic curve for the welded Ag and ZnO NW device under forward bias condition. The scattered points and the continuous curves are corresponding to experimental data points and theoretical fittings, respectively. b) Energy band diagram of Au and ZnO junction showing Schottky junction. Φ_i is the energy barrier for electrons (blue dots) transferring from ZnO to Au, whereas Φ_B is Schottky barrier height for the electrons flowing in the opposite direction. *w* is the extension of the depletion layer corresponding to the bend part of the energy bands.

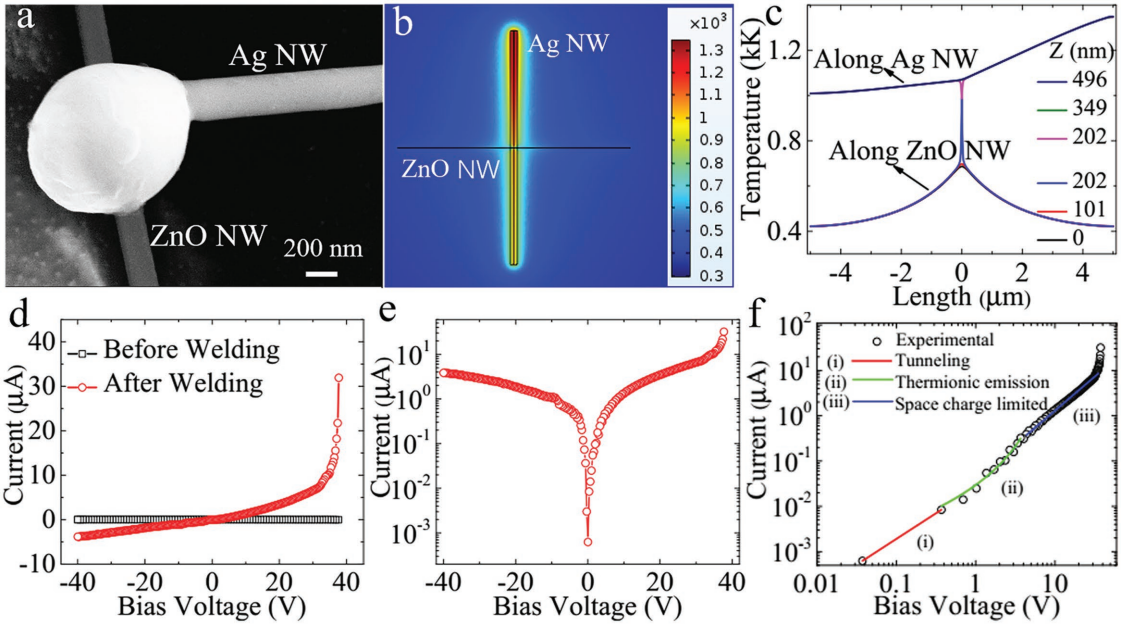

Figure 4. Welding of Ag and ZnO NWs with Ag NW on top and its electrical properties. a) SEM image of the welded ZnO and Ag NW junction. The dotted red lines represent the initial (before welding) orientation of the NWs. b) 2D plot of temperature distribution when the laser beam ($P = 30$ mW) is focused at one end of the Ag NW. The color bar corresponds to temperature in Kelvin (K) scale. c) Line plot of temperature distribution along the NWs at different height from the top surface of the substrate ($Z = 0$). d) Current–voltage characteristic curve for the welded system. e) Semilog plot of current–voltage characteristic curve. f) Logarithmic plot of current–voltage characteristic curve.

shows three distinct regions with different conduction mechanisms. For the applied bias voltage $V < 1$ V, the charge transport mechanism is speculated to be dominated by the tunneling process[46,47] which can be attributed to the barrier height Φ_i depicted in the energy band diagram of the Au–ZnO junction (see Figure 3b).[48] For the applied bias voltage ranging from 1 V to about 7 V, it is observed that current increases exponentially with voltage indicating that the transport mechanism is dominated by thermionic emission, which is also shown in the band diagram (see Figure 3b).[47,48] For the bias voltage ranging from 7 V to about 36 V, the slope of the linear fit of the I–V curve turns out to be around 2, which indicates that current is proportional to V^2. This higher power dependence suggests a space-charge limited current (SCLC) transport mechanism.[46] The SCLC transport is attributed to the charge traps distributed in both NWs and the Au electrodes.[49] With further increase of applied bias voltage up to 40 V, the slope increases to 5, which indicates that SCLC transport mechanism dominates at this voltage range also.[50] This SCLC transport mechanism is a typical behavior observed in wide bandgap semiconductors with single-carrier injection such as n-ZnO/p-Si structure.[41] It can also be mentioned that a downward bending of the I–V curve as expected in case of a series resistance is not observed for the applied maximum voltage of + 40 V.[51]

2.2. Nanowelding with Ag Nanowire on Top

An Ag ($D = 294$ nm) and a ZnO ($D = 202$ nm) NWs are welded by keeping Ag NW on top and using a focused CW laser as mentioned in the previous section (see Figure 1b). The SEM image of the welded junction of the ZnO and Ag NWs is shown in **Figure 4**a. The Ag and ZnO NWs cannot be welded by applying the same approach as mentioned in the previous section where ZnO NW is on top of the Ag NW. If the same method is followed as before, it is observed that only the Ag NW melts but ZnO NW does not, which results in Ag NW breaking apart without forming any contact with the ZnO NW. To address this issue, a different approach has been implemented. Instead of targeting laser shot at the crossing point of the NWs, the laser is focused at one end of the Ag NW. In this method, the Ag NW melts and forms a spherical ball at the end of the NW.[52] Multiple laser shots are used on this spherical ball until it reaches the ZnO NW and stick to it. In this case, the ZnO NW does not melt, but the contact area becomes large enough for effective electric connectivity. The laser power used for the welding is 30 mW. The polarization is fixed in such a way that the corresponding electric field is parallel to the long axis of Ag NW. The 2D plot of temperature distribution (shown in Figure 4b) and line plots of temperature distribution along the NWs at different heights from the top surface of the Au electrode (shown in Figure 4c) show that the maximum temperature at the end of the Ag NW is about 1300 K, which is just above the melting point of Ag. Therefore, the end of the Ag NW melts and recoils toward the ZnO NW when the laser shot is focused at the end of the Ag NW, and this process is repeated until it reaches the ZnO NW.

Thereafter, the other ends of the Ag and ZnO NWs are welded on the Au electrode following the same method as described in the previous section, and the I–V characteristic curve for the welded system is recorded. The curve obtained for the before welding system is also plotted for comparison in Figure 4d. To

distinguish the change of current profile due to the change of bias voltage polarity, semilog plot of *I–V* characteristic curve is shown in Figure 4e, and toward understanding the transport mechanisms, the log plot of the *I–V* characteristic curve is fitted theoretically considering three different transport mechanisms for three different applied voltage regime (see Figure 4f). These three figures show that the characteristic current profiles and the underlined transport mechanisms for this device are similar to the one obtained previously. This behavior is expected as the devices are essentially same, and only the method of fabrication is different. In this regard, it can be mentioned that the maximum current obtained in this case is about 30 μA which is comparable to the value obtained for the previous device. This indicates that the welding quality of this device is akin to the one when ZnO NW is kept on top for welding. Therefore, this method is import as the fabrication is relatively easier than the previous one.

2.3. Nanowelding of ZnO Nanowire on Au Electrodes

Two ends of a single ZnO NW ($D = 274$ nm) are welded on two Au electrodes to obtain back-to-back Schottky junctions (see Figure 1c). SEM image of a welded ZnO NW on Au electrodes is shown in **Figure 5**a. The zoomed in images of ZnO and Au junctions (marked by red rectangles) are shown in the insets. It can be observed from the figures that the ZnO NW and the Au thin film melt and stick together. The CW laser beam ($P = 70$ mW) is focused on the ends of the NW to weld the ZnO NW with the Au thin film. The laser light gets absorbed by the ZnO NW and the Au thin film. Therefore, the temperature of the system increases due to this conversion of light energy to thermal energy. The corresponding simulated 2D plot of temperature distribution shows that the maximum temperature at the contact point of the ZnO NW and the Au substrate is about 2200 K, therefore both the ZnO NW and the Au substrate melt (see Figure 5b). In this regard, it can be mentioned that the welding of ZnO NW on Au substrate is not as sensitive to the incident power as in case of welding ZnO NW with Ag NW.

Thereafter, the current–voltage characteristic curve for ZnO NW welded on Au electrodes is recorded using a picoammeter attached with two tungsten microprobes (see Figure 5c). It can be observed from this curve that the maximum current value is about 7 μA, which is about one-sixth of the current obtained for one Schottky junction. It can also be noted that the current is more or less symmetric for forward and reverse bias voltage. This effect can be better understood from the energy band diagram shown in Figure 5d. The symmetric nature of the current profile is attributed to the fact that the barrier is symmetric for both polarities of the applied bias voltage.

It should also be noted that there is little difference in rectification property under reverse bias condition for this back-to-back Schottky junction consisting of only Au–ZnO junctions with the single Schottky junction devices consisting of Au-ZnO and Ag-ZnO junctions, which indicates that the rectification property is determined by the Au–ZnO junction barrier in case of the single Schottky junction devices.

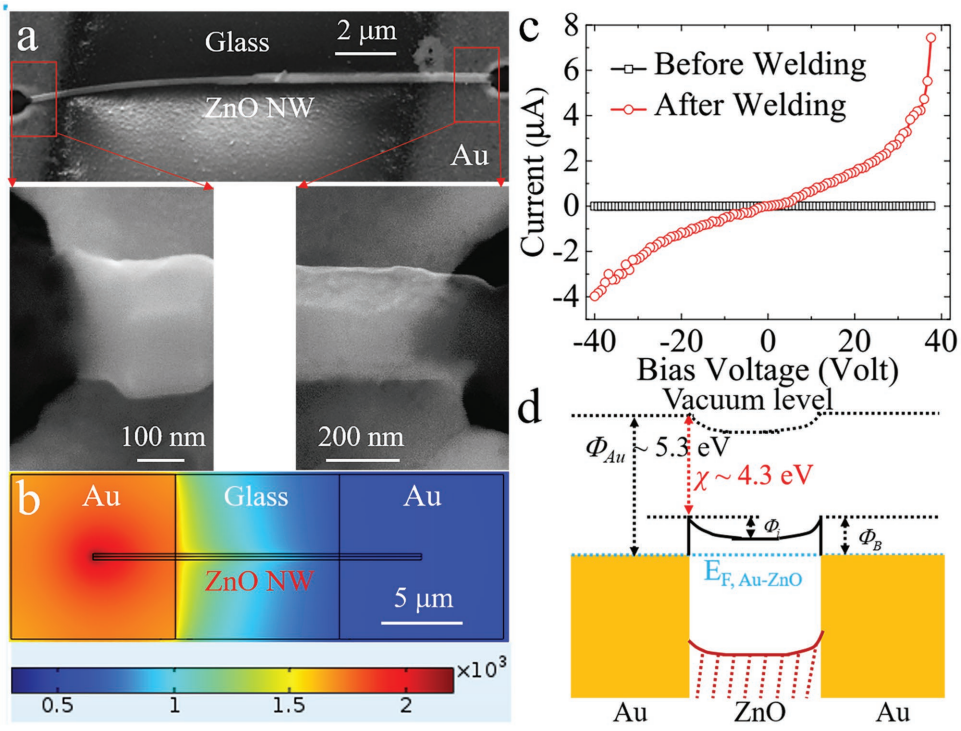

Figure 5. Welding of ZnO NW on Au electrodes and its electrical properties. a) SEM image of a welded ZnO NW on Au electrodes. The zoomed in images of ZnO and Au junctions (marked by red rectangles) are shown in the insets. b) Simulated 2D plot of temperature distribution when laser beam ($P = 70$ mW) is focused at one end of the ZnO NW placed on Au substrate. The color bar corresponds to temperature in Kelvin (K) scale. c) Current–voltage characteristic curves for the ZnO NW before and after welding on Au electrodes. d) Energy band diagram for the ZnO NW welded on Au electrodes.

2.4. Nanowelding of Ag Nanowires on Au Electrodes

For the completeness of the comparative studies, two Ag NWs are welded together and also welded on Au substrate (see Figure 1d). The SEM image of the welded junction of two Ag NWs is shown in **Figure 6**a. The diameter of the bottom and the top NWs are 326 and 260 nm, respectively. The length of both the NWs is about 10 µm. Parallel polarization of the incident laser ($P = 120$ mW) is used for welding the junction of the NWs. Corresponding to this incident laser power and polarization, the simulated 2D (for $Z = 326$ nm) and 1D (for varying Z) plots of temperature distribution along the Ag NWs are shown in Figure 6b,c, respectively. These simulated results show that the maximum temperature of the top NW is close to the melting point of bulk Ag, whereas it is much lower for the bottom NW. Therefore, it can be concluded that the top NW melts and gets welded with the bottom NW. The required laser power to weld Ag NW on Au substrate is 60 mW. The corresponding simulated 2D and 1D plots of temperature distribution are shown in Figure 6d,e, respectively. It can be observed from these plots that the maximum temperature is about 1200 K, and therefore both Ag NW and Au substrate melt and get welded. In this regard, it can be mentioned that the welding of Ag NW on Au substrate is not as sensitive to the incident laser power as in case of welding the junction of the two Ag NWs. Effective welding of Ag NW on Au substrate can be achieved even if the incident laser power is a few mW more than the required power, whereas the welding of the junction of the two Ag NWs fails for the same.

The recorded current–voltage characteristic curves for Ag NWs before and after welding at three places (the junction of the two Ag NWs and two ends Ag NWs on two different Au electrodes) show that the conductivity increases drastically after welding (see Figure 6f). All three welded junctions being ohmic type, the I–V curve comes out to be a straight line unlike the cases with Schottky junctions.

3. Conclusion

In conclusion, a comparative study of different types of electronic nanodevices fabricated by plasmonic-enhanced targeted nanowelding of various combinations of Ag and ZnO NWs on Au substrate using focused CW laser has been presented. Out of the two different approaches, which have been persuaded to fabricate devices consisting of one Schottky junction and two ohmic junctions, in one approach, melting points of both ZnO and Ag NWs are reached simultaneously at the junction by keeping the ZnO NW on top, and in the other approach, only Ag NW is melted from one end and welding is attained with ZnO NW. The current values obtained for both these devices corresponding to the maximum applied bias voltage 40 V are 42 and 30 µA, which indicates that superior welding quality has been obtained for both devices. Back-to-back Schottky junctions have been fabricated by welding two ends of a ZnO NW on two different Au electrodes. The current value obtained for this device corresponding to the maximum applied bias voltage 40 V is 7 µA, which is one sixth of the maximum current obtained for a single Schottky junction. For completeness of this comparative study, a device comprising of three ohmic contacts has also been fabricated by welding two Ag NWs on Au electrodes. These

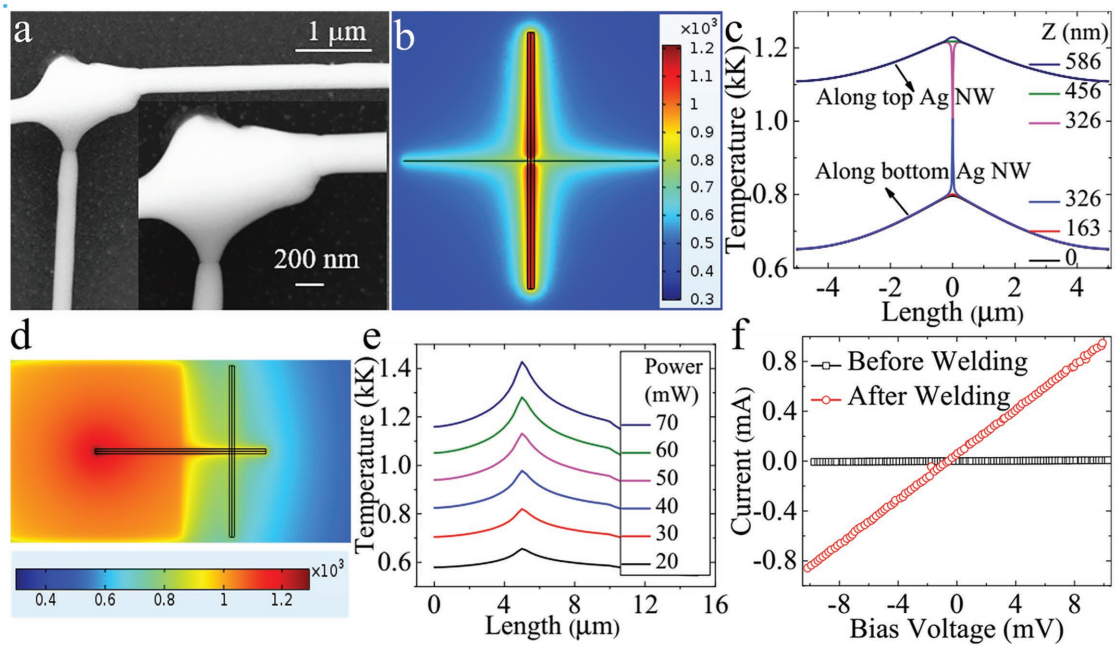

Figure 6. Welding of Ag NWs and its electrical properties. a) SEM image of a welded junction of two Ag NWs. The dotted red lines represent the initial (before welding) orientation of the NWs. The inset shows the zoomed in image of the welded junction. b) 2D plot of temperature distribution along the Ag NWs for incident laser power 120 mW and corresponding to $Z = 326$ nm plane. c) Temperature distribution along the Ag NWs corresponding to different planes. d) 2D plot of temperature distribution when the incident laser beam ($P = 60$ mW) is focused at the end of the Ag NW placed on Au electrode. e) 2D plot of temperature distribution along the Ag nanowire placed on Au electrodes for different incident laser power. f) Current–voltage characteristic curves for Ag NWs before and after welding on Au electrodes.

welding techniques can be potentially used in manufacturing and repairing mechanical, photonic, and electronic nanodevices.

4. Experimental Section

Arranging Ag and ZnO NWs on Au Electrodes: Microgap electrodes using sputter etching with a focused ion beam are fabricated on a 100 nm thick gold film deposited on the silica substrate. The gap between two adjacent electrodes is kept about 10 µm. The Ag (synthesized by a self-seeding approach)[53] and the ZnO (synthesized following metalorganic vapor-phase epitaxial growth technique)[54] NWs are placed between two adjacent Au electrodes in such a way that they make a plus sign with one end of each of the NWs is on a different Au electrode. Two nanofiber probes were used for picking and placing these NWs. In order to ensure good contacts between the NWs and the electrodes, NWs were welded on the electrodes by laser shots. The welded parts are depicted as hemispheres at the ends of NWs in Figure 1a.

Current–Voltage Characteristic Curve Measurement: The apparatus for current–voltage characteristic curve measurement includes a source-meter (Keithley 2602) and two tungsten microtapers. Two tungsten microtapers are touched on the electrodes connected with the NWs, and the source-meter is used to scan the voltage and its corresponding current to obtain the *I–V* characteristic curve.

Simulation of Electromagnetic Field Distribution: Commercial finite-difference time-domain (FDTD) and COMSOL software packages were used to calculate the temperature distribution along the NWs corresponding to various incident laser power and polarization. The total power (P_t) absorbed by the NWs was obtained using FDTD software. Thereafter, this P_t value was used as heat source to obtain the temperature distribution along the NWs using commercial COMSOL software. 3D FDTD method (FDTD Solutions v8.13, Lumerical) was used to obtain the electromagnetic field distribution with perfectly matched layers as absorbing boundary conditions. The mesh size across the NW cross-section and along the NW axis was taken as 1.5 and 50 nm, respectively. A Gaussian light source (λ = 532 nm) was considered for the simulations.

Simulation of Temperature Distribution: From the FDTD results, the electric field distribution in the NWs is extracted, and the heat power volume density Q is calculated using the relation $Q = \frac{1}{2}\varepsilon_0 \omega \mathrm{Im}(\varepsilon_r)|E|^2$, where ε_0, ω, ε_r, and E are free space permittivity, angular frequency of the incident light, relative permittivity, and electric field, respectively.[55] Thereafter, this Q value is used as heat source in commercial COMSOL Multiphysics software for simulating the temperature distribution along the NWs. The thermal conductivities of silica and air are taken from the COMSOL library, and thermal conductivities of the Ag and ZnO NWs are considered to be 170[56] and 50 Wm^{-1} K^{-1}, respectively.[57]

Supporting Information

Supporting Information is available from the Wiley Online Library or from the author.

Acknowledgements

This work was supported by the National Key Research and Development Program of China (2017YFA0205700 and 2017YFE0100200) and the National Natural Science Foundation of China (Grant Nos. 61425023, 61575177, and 61775194).

Conflict of Interest

The authors declare no conflict of interest.

Keywords

Ag nanowires, photothermal effect, Schottky junctions, ZnO nanowires

Received: December 5, 2017
Revised: January 23, 2018
Published online: February 12, 2018

[1] H. Lee, W. Manorotkul, J. Lee, J. Kwon, Y. D. Suh, D. Paeng, C. P. Grigoropoulos, S. Han, S. Hong, J. Yeo, S. H. Ko, *ACS Nano* **2017**, *11*, 12311.
[2] J. Bao, D. C. Bell, F. Capasso, J. B. Wagner, T. Mårtensson, J. Trägårdh, L. Samuelson, *Nano Lett.* **2008**, *8*, 836.
[3] C. S. Lao, J. Liu, P. Gao, L. Zhang, D. Davidovic, R. Tummala, Z. L. Wang, *Nano Lett.* **2006**, *6*, 263.
[4] M. S. Arnold, P. Avouris, Z. W. Pan, Z. L. Wang, *J. Phys. Chem. B* **2003**, *107*, 659.
[5] J. O. Hwang, D. H. Lee, J. Y. Kim, T. H. Han, B. H. Kim, M. Park, K. No, S. O. Kim, *J. Mater. Chem.* **2011**, *21*, 3432.
[6] G. Zhu, R. Yang, S. Wang, Z. L. Wang, *Nano Lett.* **2010**, *10*, 3151.
[7] S. Bashar, C. Wu, M. Suja, H. Tian, W. Shi, J. Liu, *Adv. Opt. Mater.* **2016**, *4*, 2063.
[8] M. H. Huang, S. Mao, H. Feick, H. Yan, Y. Wu, H. Kind, E. Weber, R. Russo, P. Yang, *Science* **2001**, *292*, 1897.
[9] X. W. Sun, B. Ling, J. L. Zhao, S. T. Tan, Y. Yang, Y. Q. Shen, Z. L. Dong, X. C. Li, *Appl. Phys. Lett.* **2009**, *95*, 133124.
[10] L. Li, H. Yang, H. Zhao, J. Yu, J. Ma, L. An, X. Wang, *Appl. Phys. A* **2009**, *98*, 635.
[11] S. H. Ko, D. Lee, H. W. Kang, K. H. Nam, J. Y. Yeo, S. J. Hong, C. P. Grigoropoulos, H. J. Sung, *Nano Lett.* **2011**, *11*, 666.
[12] Z. Jia, H. Wei, D. Pan, H. Xu, *Nanoscale* **2016**, *8*, 20118.
[13] S. R. Das, Q. Nian, M. Saei, S. Jin, D. Back, P. Kumar, D. B. Janes, M. A. Alam, G. J. Cheng, *ACS Nano* **2015**, *9*, 11121.
[14] Q. Nian, M. Saei, Y. Xu, G. Sabyasachi, B. Deng, Y. P. Chen, G. J. Cheng, *ACS Nano* **2015**, *9*, 10018.
[15] H. Ditlbacher, A. Hohenau, D. Wagner, U. Kreibig, M. Rogers, F. Hofer, F. R. Aussenegg, J. R. Krenn, *Phys. Rev. Lett.* **2005**, *95*, 257403.
[16] J. H. Park, G.-T. Hwang, S. Kim, J. Seo, H.-J. Park, K. Yu, T.-S. Kim, K. J. Lee, *Adv. Mater.* **2017**, *29*, 1603473.
[17] S. Han, S. Hong, J. Ham, J. Yeo, J. Lee, B. Kang, P. Lee, J. Kwon, S. S. Lee, M.-Y. Yang, S. H. Ko, *Adv. Mater.* **2014**, *26*, 5808.
[18] G. Gonzalez-Rubio, J. Gonzalez-Izquierdo, L. Banares, G. Tardajos, A. Rivera, T. Altantzis, S. Bals, O. Pena-Rodriguez, A. Guerrero-Martinez, L. M. Liz-Marzan, *Nano Lett.* **2015**, *15*, 8282.
[19] L. Zhou, J. Lu, H. Yang, S. Luo, W. Wang, J. Lv, M. Qiu, Q. Li, *Appl. Phys. Lett.* **2017**, *110*, 081101.
[20] R. Yan, D. Gargas, P. Yang, *Nat. Photonics* **2009**, *3*, 569.
[21] A. M. Gobin, D. P. O'Neal, D. M. Watkins, N. J. Halas, R. A. Drezek, J. L. West, *Lasers Surg. Med.* **2005**, *37*, 123.
[22] X. M. Henry Huang, C. A. Zorman, M. Mehregany, M. L. Roukes, *Nature* **2003**, *421*, 496.
[23] D. P. Langley, M. Lagrange, G. Giusti, C. Jimenez, Y. Brechet, N. D. Nguyen, D. Bellet, *Nanoscale* **2014**, *6*, 13535.
[24] J. A. Spechler, C. B. Arnold, *Appl. Phys. A* **2012**, *108*, 25.
[25] E. C. Garnett, W. Cai, J. J. Cha, F. Mahmood, S. T. Connor, M. Greyson Christoforo, Y. Cui, M. D. McGehee, M. L. Brongersma, *Nat. Mater.* **2012**, *11*, 241.
[26] J. Mertens, A. Demetriadou, R. W. Bowman, F. Benz, M. E. Kleemann, C. Tserkezis, Y. Shi, H. Y. Yang, O. Hess, J. Aizpurua, J. J. Baumberg, *Nano Lett.* **2016**, *16*, 5605.
[27] L. Lin, G. Zou, L. Liu, W. W. Duley, Y. N. Zhou, *Appl. Phys. Lett.* **2016**, *108*, 203107.

[28] Q. Li, G. Liu, H. Yang, W. Wang, S. Luo, S. Dai, M. Qiu, *Appl. Phys. Lett.* **2016**, *108*, 193101.
[29] T. A. Celano, D. Hill, X. Zhang, C. W. Pinion, J. Christesen, C. J. Flynn, J. R. McBride, J. F. Cahoon, *Nano Lett.* **2016**, *16*, 5241.
[30] S. S. Yoon, D. Y. Khang, *Nano Lett.* **2016**, *16*, 3550.
[31] L. Dong, X. Tao, L. Zhang, X. Zhang, B. J. Nelson, *Nano Lett.* **2007**, *7*, 58.
[32] Y. Lu, J. Y. Huang, C. Wang, S. Sun, J. Lou, *Nat. Nanotechnol.* **2010**, *5*, 218.
[33] P. Peng, A. Hu, A. P. Gerlich, G. Zou, L. Liu, Y. N. Zhou, *ACS Appl. Mater. Interfaces* **2015**, *7*, 12597.
[34] C. F. Guo, Y. Lan, T. Sun, Z. Ren, *Nano Energy* **2014**, *8*, 110.
[35] Y. Peng, T. Cullis, B. Inkson, *Nano Lett.* **2009**, *9*, 91.
[36] Y. Yao, K. K. Fu, S. Zhu, J. Dai, Y. Wang, G. Pastel, Y. Chen, T. Li, C. Wang, T. Li, L. Hu, *Nano Lett.* **2016**, *16*, 7282.
[37] J. Bayley, D. Crossley, M. Ponting, *Metals and Metalworking: A Research Framework for Archaeometallurgy*, Historical Metallurgy Society, UK **2008**.
[38] O. Madelung, U. Rössler, M. Schulz, *Zinc Oxide (ZnO) Debye Temperature, Heat Capacity, Density, Melting Point, Vapor Pressure, Hardness*, Springer, Berlin **1999**.
[39] M. M. Menamparambath, C. Muhammed Ajmal, K. H. Kim, D. Yang, J. Roh, H. C. Park, C. Kwak, J.-Y. Choi, S. Baik, *Sci. Rep.* **2015**, *5*, 16371.
[40] R. R. Ford, J. Pritchard, *Trans. Faraday Soc.* **1971**, *67*, 216.
[41] X. Li, B. Zhang, H. Zhu, X. Dong, X. Xia, Y. Cui, Y. Ma, G. Du, *J. Phys. D: Appl. Phys.* **2008**, *41*, 035101.
[42] K. Ellmer, A. Klein, B. Rech, *Transparent Conductive Zinc Oxide*, Springer, Berlin **2008**.
[43] H. L. Mosbacker, Y. M. Strzhemechny, B. D. White, P. E. Smith, D. C. Look, D. C. Reynolds, C. W. Litton, L. J. Brillson, *Appl. Phys. Lett.* **2005**, *87*, 012102.
[44] F. Yan, Y. Wang, J. Zhang, Z. Lin, J. Zheng, F. Huang, *ChemSusChem* **2014**, *7*, 101.
[45] A. Di Bartolomeo, *Phys. Rep.* **2016**, *606*, 1.
[46] C. Y. Liu, H. Y. Xu, J. G. Ma, X. H. Li, X. T. Zhang, Y. C. Liu, R. Mu, *Appl. Phys. Lett.* **2011**, *99*, 063115.
[47] F. Gao, M. M. Morshed, S. B. Bashar, Y. Zheng, Y. Shi, J. Liu, *Nanoscale* **2015**, *7*, 9505.
[48] S. M. Sze, K. N. Kwok, *Physics of Semiconductor Devices*, Wiley, Hoboken, New Jersey, USA **2007**.
[49] F. Gao, D. Zhang, J. Wang, H. Sun, Y. Yin, Y. Sheng, S. Yan, B. Yan, C. Sui, Y. Zheng, Y. Shi, J. Liu, *Appl. Phys. Lett.* **2016**, *108*, 261103.
[50] J. B. Fedison, T. P. Chow, H. Lu, I. B. Bhat, *Appl. Phys. Lett.* **1998**, *72*, 2841.
[51] A. Di Bartolomeo, F. Giubileo, G. Luongo, L. Iemmo, N. Martucciello, G. Niu, M. Fraschke, O. Skibitzki, T. Schroeder, G. Lupina, *2D Mater.* **2017**, *4*, 015024.
[52] S. Dai, Q. Li, G. Liu, H. Yang, Y. Yang, D. Zhao, W. Wang, M. Qiu, *Appl. Phys. Lett.* **2016**, *108*, 121103.
[53] Y. Sun, Y. Xia, *Adv. Mater.* **2002**, *14*, 833.
[54] W. I. Park, D. H. Kim, S.-W. Jung, G.-C. Yi, *Appl. Phys. Lett.* **2002**, *80*, 4232.
[55] X. Chen, Y. Chen, M. Yan, M. Qiu, *ACS Nano* **2012**, *6*, 2550.
[56] Z. Cheng, L. Liu, S. Xu, M. Lu, X. Wang, *Sci. Rep.* **2015**, *5*, 10718.
[57] X. Wu, J. Lee, V. Varshney, J. L. Wohlwend, A. K. Roy, T. Luo, *Sci. Rep.* **2016**, *6*, 22504.

